Magnetic properties of $PdAs_2O_6$: A dilute spin system with an unusually high Néel temperature

M. Reehuis,[1] T. Saha-Dasgupta,[2] D. Orosel,[3] J. Nuss,[3] B. Rahaman,[2,*] B. Keimer,[3] O. K. Andersen,[3] and M. Jansen[3]

[1]*Helmholtz-Zentrum Berlin für Materialien und Energie, D-14109 Berlin, Germany*

[2]*S. N. Bose National Center for Basic Sciences, Salt Lake, Kolkata 700098, India*

[3]*Max Planck Institute for Solid State Research, D-70569 Stuttgart, Germany*

(Received 27 January 2012; revised manuscript received 6 March 2012; published 23 March 2012)

The crystal structure and magnetic ordering pattern of $PdAs_2O_6$ were investigated by neutron powder diffraction. While the magnetic structure of $PdAs_2O_6$ is identical to that of its isostructural 3*d* homologue $NiAs_2O_6$, its Néel temperature (140 K) is much higher than that of $NiAs_2O_6$ (30 K). This is surprising in view of the long distance and indirect exchange path between the magnetic Pd^{2+} ions. Density-functional calculations yield insight into the electronic structure and the geometry of the exchange-bond network of both $PdAs_2O_6$ and $NiAs_2O_6$, and provide a semiquantitative explanation of the large amplitude difference between their primary exchange interaction parameters.

DOI: 10.1103/PhysRevB.85.115118 PACS number(s): 75.25.−j, 75.50.Ee, 61.05.fm, 71.20.Ps

I. INTRODUCTION

The magnetic properties of transition-metal compounds with 3*d* valence electrons have been one of the central research themes in solid-state physics for the past three decades. In view of the interplay between magnetism and high-temperature superconductivity, particular attention has been focused on oxides and arsenides. Recently, the electronic structure and ordering phenomena of transition-metal compounds with 4*d* and 5*d* valence electrons (such as ruthenates and iridates) have also captured much attention. The electronic correlations in these materials are generally weaker than those of their 3*d* counterparts, while the spin-orbit coupling is stronger. The quantitative description of the influence of these parameters on the electronic phase behavior of *d*-electron compounds is an important topic of current research. Here we report on a detailed investigation of the magnetic properties of $PdAs_2O_6$, a recently synthesized[1] electrically insulating compound with a magnetic lattice of Pd^{2+} ions in the electron configuration $4d^8$. We compare our results to the isostructural compound $NiAs_2O_6$, which is based on Ni^{2+} ions with the same number of electrons in the 3*d* shell.

$PdAs_2O_6$ crystallizes in the $PbSb_2O_6$ structure with Pd^{2+} and As^{5+} ions segregated into different layers (Fig. 1). The octahedral coordination of Pd^{2+} in this structure is unusual, because divalent palladium shows a strong preference for square-planar coordination, which is associated with a diamagnetic ground state. Only a few examples of sixfold-coordinated Pd^{2+} compounds are known, including the ambient- and high-pressure polymorphs of PdF_2 as well fluoro-palladates of composition $MPdF_4$ (M = Ca,Cd,Hg) and $CsPd_2F_5$.[2] These compounds are paramagnetic at high temperatures and tend to order antiferromagnetically upon cooling. In accord with this trend, magnetic susceptibility measurements on $PdAs_2O_6$ showed paramagnetic behavior at room temperature and an antiferromagnetic phase transition at the Néel temperature $T_N \sim 150$ K.[1] This behavior is qualitatively analogous to that of the isostructural 3*d* homologues $MnAs_2O_6$, $CoAs_2O_6$, and $NiAs_2O_6$, which also show antiferromagnetic ordering with $T_N = 13$, 20, and 30 K, respectively.[3] However, the much higher Néel temperature of $PdAs_2O_6$ is surprising, especially because the PdO_6 octahedra do not share vertices, edges, or faces. The exchange paths connecting neighboring Pd^{2+} ions are therefore long and involve at least two bridging oxygen sites.

In order to elucidate the microscopic origin of this surprising behavior, we have used neutron diffraction to determine the magnetic structure of $PdAs_2O_6$, which turned out to be identical to that of the 3*d* homologues (Sec. II). This implies similar networks of exchange bonds in both sets of compounds. We employed density-functional calculations to obtain insights into the electronic structure of $PdAs_2O_6$ and $NiAs_2O_6$, and specifically into the origin of the exchange paths (which turned out to be hopping via As dimers) and of the large amplitude difference of the primary exchange interaction parameters (Sec. III). A model based on these interactions yields an excellent description of the magnetic susceptibilities of both compounds.

II. NEUTRON DIFFRACTION

A. Experimental details

A powder sample of $PdAs_2O_6$ of weight ∼3 g was prepared using the starting materials PdO (99.9% metals basis, Alfa Aesar) and As_2O_5 (99.9%, Alfa Aesar) in the molecular ratio 1 : 1.1, as described earlier.[1] The mixed powder was pressed into pellets and dried in evacuated silica tubes for 12 h at 373 K. Then the evacuated silica tubes were heated up to 973 K at a rate of 100 K/h. The hygroscopic and air-sensitive powder of $PdAs_2O_6$ was obtained after an annealing process of about 100 h. Measurements of the magnetic susceptibility and specific heat were carried out in the temperature range between 5 and 300 K (Fig. 2). Both quantities show anomalies indicative of antiferromagnetic ordering of the Pd sublattice at 140 K, in agreement with prior work.[1]

In order to investigate the crystal and magnetic structure of $PdAs_2O_6$, a neutron diffraction experiment was carried out at the research reactor FRM-II in Garching. Neutron powder patterns were collected with the instrument SPODI at 5 and 200 K in the 2θ range 4°–160°. This instrument uses a germanium monochromator (reflection 551) selecting the neutron wavelength $\lambda = 1.5476$ Å. The refinements of the crystal and magnetic structure were carried out with the program

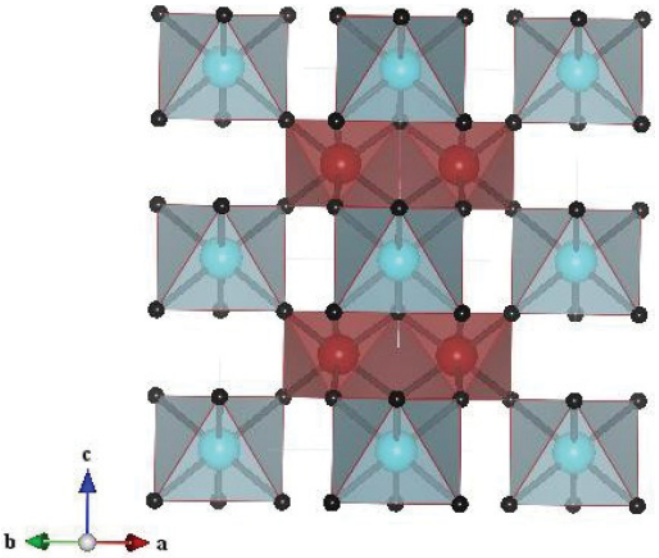

FIG. 1. (Color online) Crystal structure of $A\mathrm{As_2O_6}$ (A = Pd,Ni) showing the three-dimensional network of $\mathrm{AO_6}$ and $\mathrm{AsO_6}$ octahedra. The brown (dark gray) colored balls denote A atoms, and the cyan (light gray) colored balls represent As atoms. Small black colored balls at the corners of the octahedra are O atoms.

FULLPROF.[4] We used the nuclear scattering lengths b (Pd) = 5.91 fm, b(As) = 6.58 fm, and b(O) = 5.805 fm.[5] The magnetic form factors of the magnetic ions were taken from Ref. 6.

B. Crystal structure of $\mathrm{PdAs_2O_6}$

The crystal structure of $\mathrm{PdAs_2O_6}$ was recently refined from x-ray powder diffraction data in the trigonal $\mathrm{PbSb_2O_6}$-type structure (space group $P\bar{3}1m$, No. 162), where the Pd, As, and O atoms are in the Wyckoff positions $1a$(0,0,0), $2d(\frac{1}{3},\frac{2}{3},\frac{1}{2})$, and $6k(x,0,z)$, respectively.[1] The same space group was found earlier for the compounds $\mathrm{MnAs_2O_6}$, $\mathrm{CoAs_2O_6}$, and $\mathrm{NiAs_2O_6}$ containing $3d$-metal ions.[3] From our neutron powder diffraction data taken at the lower temperatures 5 and 200 K (Fig. 3), the trigonal space group $P\bar{3}1m$ was confirmed. For the Rietveld refinements, we used data in the extended 2θ range from 4° up to 146°. A total of 14 parameters were refined: an overall scale factor, five profile function parameters, the zero point, two lattice constants, the positional parameters x and z of the oxygen atom, as well as three isotropic thermal parameters. The powder sample contained small amounts of the binary oxide PdO, which crystallizes in the tetragonal space group $P4_2/mmc$.[7] Therefore, the overall scale factor of PdO was additionally allowed to vary during the refinements.

In Table I, the results of the refinements are compared with those of the x-ray study carried out earlier at room temperature.[1] Here it can be seen that the positional parameters of the oxygen atoms determined at 5 and 200 K are in good agreement, indicating that the structural changes between the magnetically ordered and the paramagnetic states are weak. Only a slight reduction of 0.0036 Å (about 6 σ) could be observed for the Pd-O bond length in the $\mathrm{PdO_6}$ octahedra. In contrast, the distances between the As and O atoms are practically unchanged (Table I). The value

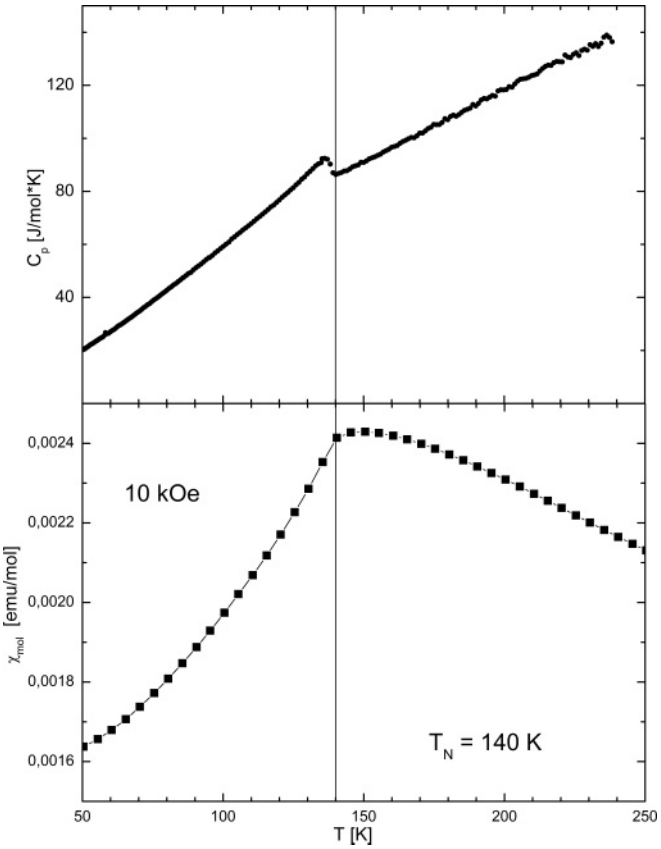

FIG. 2. Temperature dependence of the specific heat and the inverse magnetic susceptibility of $\mathrm{PdAs_2O_6}$.

d(As-O) = 1.8281(6) Å (at 200 K) found for $\mathrm{PdAs_2O_6}$ is in very good agreement with the values of other arsenates containing $3d$-metal ions: d(As-O) = 1.827(4) Å ($\mathrm{NiAs_2O_6}$), d(As-O) = 1.830(3) Å ($\mathrm{CoAs_2O_6}$), d(As-O) = 1.826(2) Å ($\mathrm{MnAs_2O_6}$), and d(As-O) = 1.826(1) Å ($\mathrm{CdAs_2O_6}$).[3,8] All of these values are in agreement with d(As-O) = 1.82 Å calculated for an $\mathrm{AsO_6}$ octahedron given by Shannon.[9] In Table I, it can be seen that the structural parameters obtained at 200 and 300 K show relatively large discrepancies, despite the fact that both data sets were collected in the paramagnetic phase. This can be ascribed to the larger scattering power of the O atoms in neutron diffraction, with the result that the O positions can be determined more reliably. Furthermore, the shortest oxygen contact d(O-O) = 2.308(3) Å was found to be implausibly short in the x-ray study.[1] From our neutron diffraction study, we found the larger values d(O-O) = 2.3757(12) Å at 5 K and d(O-O) = 2.3726(12) Å at 200 K, respectively. The value d(O-O) = 2.410(3) Å found for $\mathrm{NiAs_2O_6}$ is slightly larger,[3] while the As-O-bond lengths d(As-O) = 1.827(4) Å ($\mathrm{NiAs_2O_6}$) and d(As-O) = 1.8281(6) Å ($\mathrm{PdAs_2O_6}$) are practically the same in both compounds. The cell volume of the Ni compound [V = 86.97(3) Å^3] is much smaller than that of the Pd compound [V = 93.698(2) Å^3]. This is due to the fact that the ionic radius of $\mathrm{Pd^{2+}}$ is larger than that of $\mathrm{Ni^{2+}}$. In order to keep the As-O-bond lengths almost constant in the $\mathrm{AsO_6}$ octahedra, the bond angle ∠(O-As-O) increases from 169.91(3)° in $\mathrm{PdAs_2O_6}$ to 173.23(12)° in $\mathrm{NiAs_2O_6}$.

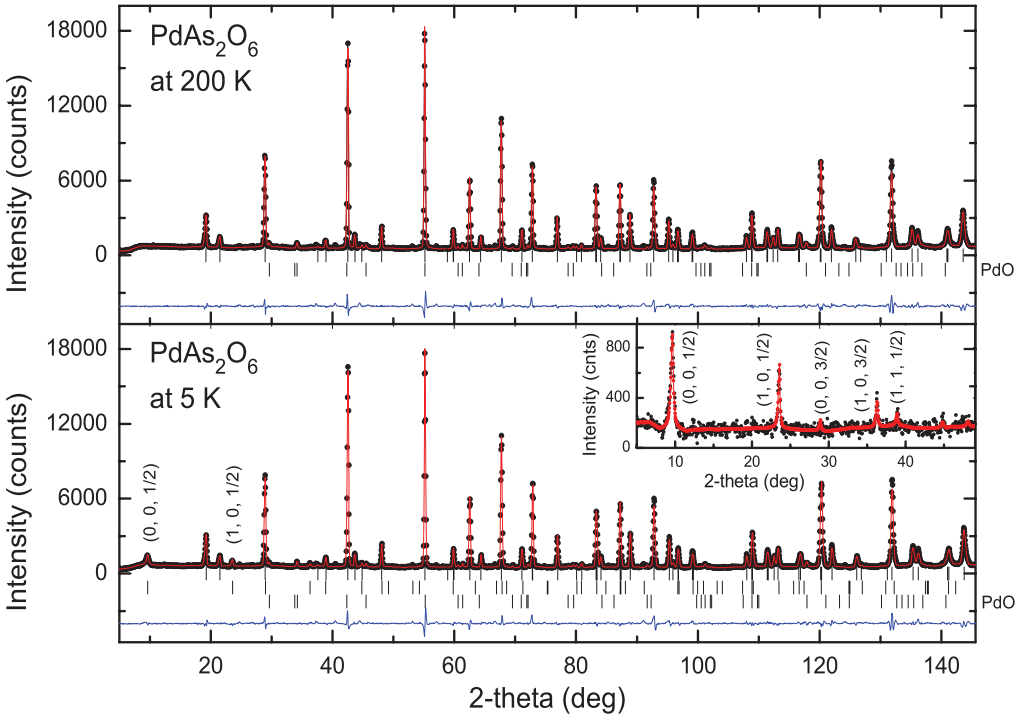

FIG. 3. (Color online) Neutron powder diffraction data of $PdAs_2O_6$ collected at 5 and 200 K. The crystal structure was refined in the hexagonal space group $P\bar{3}1m$. The calculated patterns (red lines) are compared to the observed ones (black circles). In the lower part of each diagram, the difference pattern (blue) as well as the positions of the nuclear reflections of $PdAs_2O_6$ and the impurity phase PdO (black bars) are shown. For the powder pattern collected at 5 K, the positions of the magnetic reflections of $PdAs_2O_6$ are also shown. The inset shows the magnetic Bragg reflections of $PdAs_2O_6$, obtained from the difference between the diffraction patterns at 5 and 200 K.

TABLE I. Results of Rietveld refinements of the neutron powder diffraction data ($\lambda = 1.5476$ Å) for the nuclear structure of $PdAs_2O_6$ at 5 and 200 K. The lattice constants, positional, and isotropic thermal parameters as well as the bond distances and angles within the AsO_6 and PdO_6 units are compared with the values obtained earlier at room temperature from x-ray powder diffraction data ($\lambda = 0.7093$ Å).[1] The residual R_N of the refinement of the crystal structure is defined as $R_N = \sum ||(F_{obs}| - |F_{calc}||/|(F_{obs}|$. The residual for the room-temperature structure (marked by $*$) was calculated with intensities rather than structure factors.[1]

	5 K	200 K	290 K
a (Å)	4.81700(4)	4.81837(5)	4.8196(1)
c (Å)	4.65618(6)	4.66014(7)	4.6646(1)
V (Å^3)	93.565(2)	93.698(2)	93.835(3)
x(O)	0.37187(15)	0.37230(16)	0.3695(7)
z(O)	0.28203(18)	0.28236(18)	0.2926(5)
B(Pd) (Å^2)	0.46(3)	0.62(3)	0.80(3)
B(As) (Å^2)	0.49(2)	0.54(2)	0.88(3)
B(O) (Å^2)	0.62(2)	0.74(2)	0.55(6)
d(Pd-O) (Å)	2.2211(6) (6×)	2.2247(6) (6×)	2.2437(20) (6×)
∠(O-Pd-O) (deg)	180 (3×)	180 (3×)	180 (3×)
	88.61(2) (6×)	88.58(2) (6×)	86.84(10) (6×)
	91.39(2) (6×)	91.42(2) (6×)	93.16(10) (6×)
d(As-O) (Å)	1.8288(6) (6×)	1.8281(6) (6×)	1.8076(23) (6×)
∠(O-As-O) (deg)	169.91(3) (3×)	169.79(3) (3×)	170.42(13) (3×)
	81.01(3) (3×)	80.92(4) (3×)	79.34(15) (3×)
	92.18(3) (3×)	92.19(3) (3×)	93.34(15) (3×)
	95.49(2) (6×)	95.57(2) (6×)	94.03(10) (6×)
d(O-O)$_{min}$ (Å)	2.3757(12)	2.3726(12)	2.308(3)
R_N	0.0241	0.0298	0.0859*

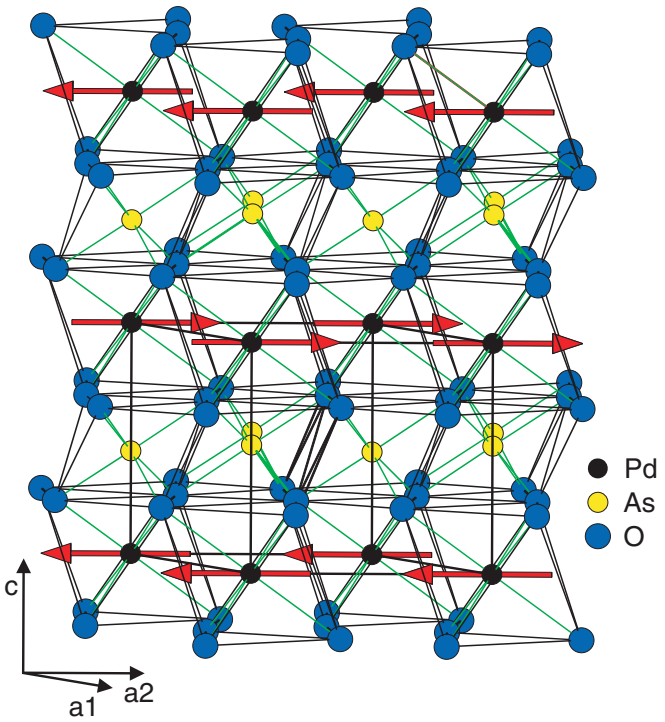

FIG. 4. (Color online) Magnetic structure of $PdAs_2O_6$. Shown are the isolated PdO_6 octahedra between the AsO_6 layers. The magnetic moments of the palladium atoms are aligned ferromagnetically within the hexagonal ab plane. Along the c direction, the moments are coupled in an antiparallel fashion, forming the sequence $+-+-$.

C. Magnetic structure of $PdAs_2O_6$

The neutron powder data recorded at 5 K show additional Bragg reflections that can be ascribed to the antiferromagnetic order of the Pd sublattice. The two prominent ones at $2\theta = 9.5^\circ$ and 23.5° can be indexed as $(0, 0, \frac{1}{2})_M$ and $(0, 1, \frac{1}{2})_M$, respectively. This suggests that the magnetic cell has a doubled c axis with a propagation vector $\boldsymbol{k} = (0, 0, \frac{1}{2})$. All further magnetic reflections were assigned indices according to $(hk\ell)_M = (hk\ell)_N \pm \boldsymbol{k}$, where M and N designate the magnetic and nuclear reflections. The same type of magnetic ordering was observed earlier for the isotypic divalent transition-metal arsenates $CoAs_2O_6$ and $NiAs_2O_6$.[3] The presence of the strong magnetic reflection $(0, 0, \frac{1}{2})_M$ indicates that the magnetic moments of the Pd atoms are aligned ferromagnetically within the hexagonal ab plane. Due to antiferromagnetic exchange interactions between the palladium moments, the ferromagnetic layers form the sequence $+-+-$ along the c axis (Fig. 4). With this model, the magnetic structure of $PdAs_2O_6$ could be successfully refined using the magnetic reflections observed in the 2θ range up to 50°. It has to be noted that the moment direction within the hexagonal plane cannot be determined from the refinements. The wave vector $\boldsymbol{k} = (0, 0, \frac{1}{2})$ keeps the full symmetry of the group $\boldsymbol{G}_k = \boldsymbol{G}$ according to magnetic group theory, and it defines the magnetic translation lattice.[10] The existence of three magnetic domains in the hexagonal basis plane prohibits an unambiguous determination of the moment direction.

TABLE II. Observed and calculated intensities of the magnetic reflections of $PdAs_2O_6$ as obtained from Rietveld refinements using the magnetic form factors of Ni^{2+} and Pd^{+}.[6] The residual R_M is defined as $R_M = \sum ||(I_{obs}| - |I_{calc}||/|(I_{obs}|$.

	I_{obs}	I_{calc} (Ni^{2+})	I_{calc} (Pd^{+})	2θ (deg)
$(0,0,\frac{1}{2})_M$	518	445	503	9.5
$(1,0,\frac{1}{2})_M$	198	205	178	23.5
$(0,0,1\frac{1}{2})_M$	9	34	25	28.8
$(1,0,1\frac{1}{2})_M$	88	87	50	36.2
$(1,1,\frac{1}{2})_M$	42	45	23	38.8
$(2,0,\frac{1}{2})_M$	30	28	11	44.8
$(1,1,1\frac{1}{2})_M$	43	28	9	48.0
$(0,0,2\frac{1}{2})_M$	2	6	2	49.1
μ_{exp} (Pd^{2+}) (μ_B)		1.87(3)	2.04(3)	
R_M		0.141	0.173	

In order to improve the refinement of the magnetic structure, we used the purely magnetic intensities obtained from the difference between the data sets collected at 5 and 200 K (inset of Fig. 2). Since the magnetic form factor of Pd^{2+} is not available, we first used the one of the Pd^{+} ion,[6] but Table II shows that the calculated intensities decrease much more strongly with increasing 2θ than the observed ones. A considerably better fit was obtained with the form factor of Ni^{2+}, which also shows a d^8 configuration. The relatively large residual $R_M = 0.141$ [defined as $R_M = \sum ||(I_{obs}| - |I_{calc}||/|(I_{obs}|$] reflects the fact that the low intensities of the magnetic reflections at high 2θ values could not be measured with good accuracy, in combination with systematic errors arising from the difference between the form factors of Pd^{2+} and Ni^{2+}.

The sublattice magnetization resulting from the refinement is $\mu = 1.92(4)\mu_B$ per Pd site, similar to the value $\mu = 2.11(3)\mu_B$ reported for $NiAs_2O_6$ (Ref. 3). While the ordered moment is consistent with the spin-only moment expected for a d^8 configuration, a fit to the magnetic susceptibility for $T > T_N$ yields a g factor larger than 2, which is indicative of an orbital contribution to the Pd moment (see Sec. III C below). The difference may in part be due to zero-point fluctuations of the magnetic moment, which reduce the ordered moment of the spin-1 system in the binary oxide NiO by $\sim$8%.[11] The zero-point reduction is possibly larger in $PdAs_2O_6$ because of the low-dimensional exchange-bond network (see Sec. III C). While these considerations suggest a small but nonzero orbital contribution to the Pd moment, measurements of the g-factor anisotropy by single-crystal neutron diffraction and/or electron-spin resonance will be required to quantify this contribution.

III. DENSITY-FUNCTIONAL CALCULATIONS

A. LDA band structure

Figure 5 shows the electronic band structure and density of states in the paramagnetic local density-functional approximation (LDA[12]) for NiAs $_2O_6$ (depicted by solid lines) and

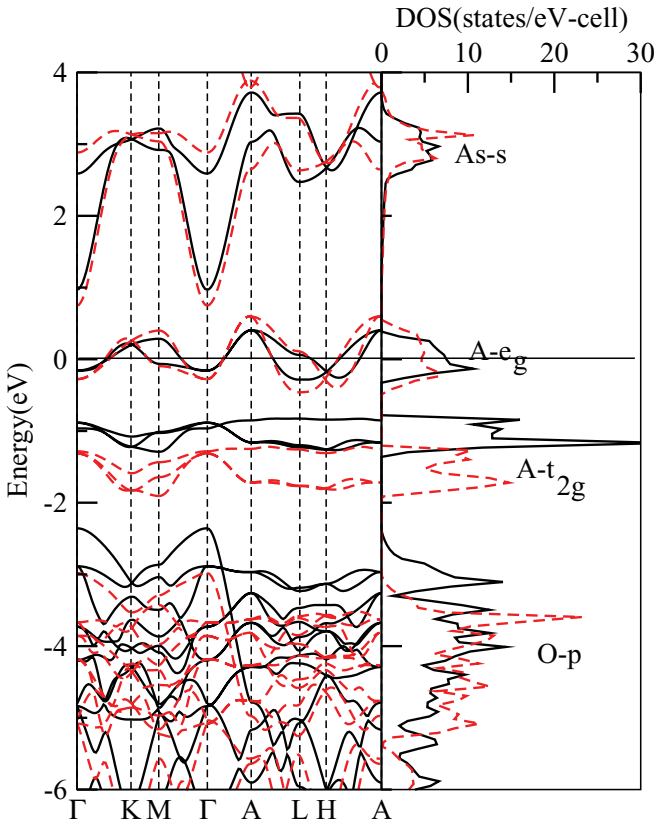

FIG. 5. (Color online) LDA band structure (left panel) and density of states (right panel) for $NiAs_2O_6$ (solid lines) and $PdAs_2O_6$ (dashed lines). The two band structures have their Fermi levels (0 eV) lined up. The bands are plotted along the high-symmetry directions of the hexagonal Brillouin zone and the densities of states have their dominating characters labeled.

for $PdAs_2O_6$ (depicted by dashed lines). The self-consistent calculations were performed with the linear muffin-tin orbital (LMTO) method[13] using $8 \times 8 \times 8$ **k** points in the Brillouin zone.

The Fermi level falls in the middle of the two narrow transition-metal (A) e_g bands. These are split above the three narrow t_{2g} bands, because the $pd\sigma$ hopping is $\sim\sqrt{3}$ times stronger than the $pd\pi$ hopping to the O p orbitals at the corners of the AO_6 octahedron. This is in accord with the labeling A^{2+}. Similarly, in accord with the labeling O^{2-} and As^{5+}, the oxygen $2p$-like bands are below and the As s- and As p-like bands are above the Fermi level. However, in terms of atomically localized orbitals (LMTOs) rather than Wannier orbitals, the bands denoted as As s in the figure have ~40% antibonding O p character, as well as some A s and O s characters. Correspondingly, around −12 eV (below the frame of the figure) there are two bands with As s and O sp bonding characters in about equal amounts.

With the bands lined up at the Fermi level, the t_{2g} and p bands lie lower in the Pd than in the Ni compound. This is because $4d$ orbitals have a larger extent and therefore larger hopping integrals to O p than do $3d$ orbitals. For the same reason, the e_g band is about 1.4 times wider in the Pd than in the Ni compound.

Inclusion of the Coulomb interaction beyond the LDA splits the e_g bands and leads to insulating solutions, as we have checked through LDA + U (Ref. 14) calculations. For the present purpose of calculating and understanding the magnetic properties, it is more convenient to start from the localized description and treat the hopping, t, to order t^2/U.

B. Pd e_g Wannier orbitals, low-energy tight-binding Hamiltonian, and magnetic interactions

We therefore construct a low-energy Hubbard Hamiltonian. Since the LDA e_g band is narrow and well separated from all other bands, we can limit the one-electron Hilbert space to that of the two A-centered Wannier orbitals, $3z^2 - r^2$ and $x^2 - y^2$, describing this band. When using the N MTO downfolding method, we thus kept the A e_g degrees of freedom as active, and we downfolded the rest. The Wannier orbitals are finally obtained by symmetrically orthonormalizing the

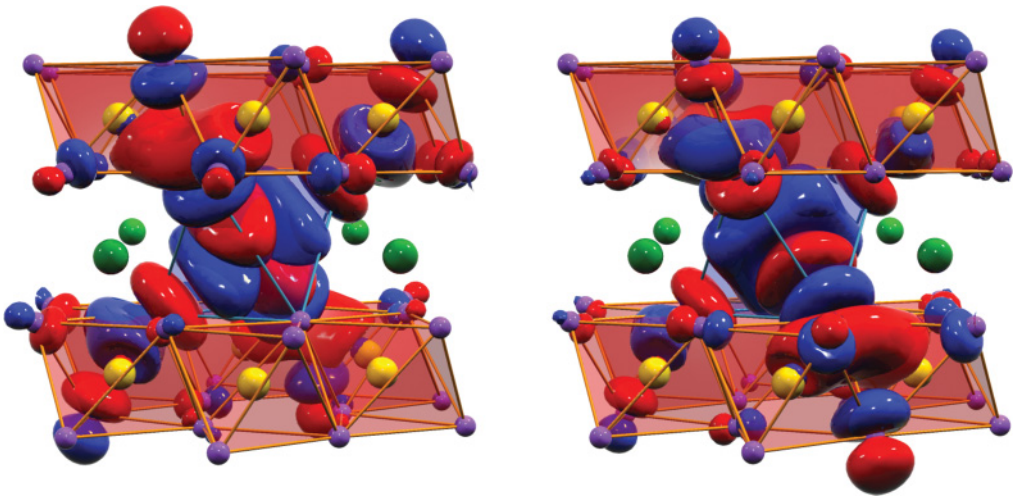

FIG. 6. (Color online) The $x^2 - y^2$ (left panel) and $3z^2 - r^2$ (right panel) Wannier orbitals, which span the LDA Pd e_g bands of $PdAs_2O_6$. Plotted are orbital shapes (constant-amplitude surfaces) with lobes of opposite signs colored red (dark) and blue (light). For clarity, the central PdO_6 octahedron is given a blue skin and all AsO_6 octahedra a red skin. Pd atoms are green, As atoms are yellow, and O atoms are violet.

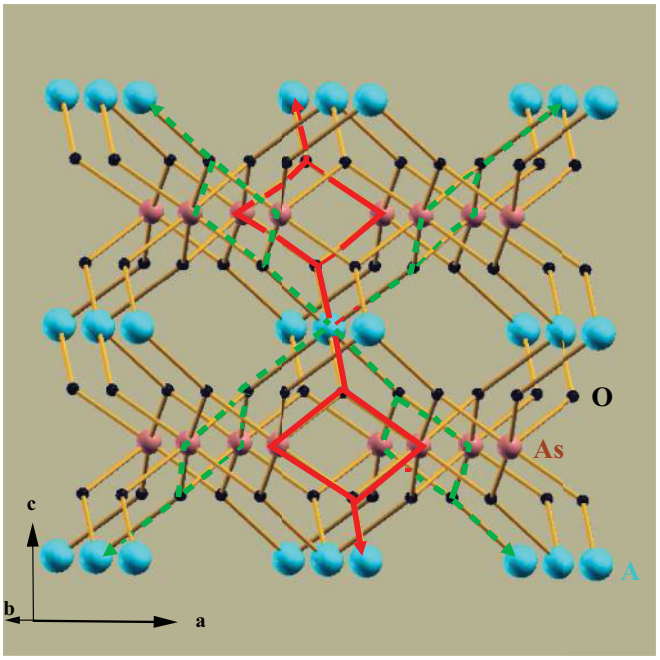

FIG. 7. (Color online) Paths of the dominant hoppings. Dashed green: between $x^2 - y^2$ orbitals (see the left-hand side of Fig. 6) on third-nearest A neighbors. Solid red: between $3z^2 - r^2$ orbitals (see the right-hand side of Fig. 6) on third-nearest A neighbors. The colors of the atoms are as in Fig. 1.

downfolded, Nth-order muffin-tin orbitals (NMTOs[15]). In the representation $H = \sum t_{im,jm'}(\hat{c}^{\dagger}_{im}\hat{c}_{jm'} + \text{H.c.})$ of the corresponding one-electron part of the Hamiltonian, $t_{im,jm'}$ is the hopping integral from orbital m on site i to orbital m' on site j.

Figure 6 shows the $x^2 - y^2$ and $3z^2 - r^2$ Wannier orbitals for $PdAs_2O_6$ as $\chi(\mathbf{r}) = \pm\text{const}$ surfaces with positive lobes colored red and negative blue. The z axis points along the Pd-O bond in the bc plane and the x and y axes point to the other oxygens in the Pd-centered octahedron. In the figure, the latter has been given a blue, transparent skin while all As-centered octahedra have been given a red, transparent skin. Pd atoms are green, As atoms yellow, and O atoms violet. Such a Pd-centered Wannier orbital has $x^2 - y^2$ or $3z^2 - r^2$ character locally, and strong $pd\sigma$ antibonding character on the neighboring oxygens. The unusual feature here is that the *back* lobes of the strongest O p characters (the four p_x and p_y tails of the $x^2 - y^2$ Wannier orbital and the two p_z tails of the $3z^2 - r^2$ Wannier orbital) bond to the sp characters on the closest *pair of As atoms* and, from there, antibond to the closest oxygen, which now belongs to a neighboring PdO_6 octahedron. As an example, the red lobe of the $x^2 - y^2$ orbital, sticking up and out toward the reader, antibonds with the blue lobe of the near p_x orbital, whose red back lobe merges together (bonds) with the red, two-center As sp bond, giving rise to a "red sausage." The latter finally antibonds with the O p orbital, which points upward toward a near Pd belonging to the upper Pd sheet (not shown in the figure). Similarly, for the $3z^2 - r^2$ orbital on the right-hand side of the figure, its red lobe, sticking down and out, antibonds with the blue lobe of the near p_z orbital, which merges with the As two-center bond into a red sausage. The latter finally induces strong p_z-like character, which points down and out toward a Pd atom in the lower Pd sheet.

These hopping paths, shown schematically in Fig. 7, are to third-nearest Pd neighbors, but only to six out of the twelve, namely to those at $\pm(0,1,1)$, $\pm(\frac{\sqrt{3}}{2},\frac{1}{2},-1)$, and $\pm(\frac{\sqrt{3}}{2},-\frac{1}{2},1)$. The e_g integrals for hopping to the third-nearest neighbors at $\pm(0,1,-1)$, $\pm(\frac{\sqrt{3}}{2},\frac{1}{2},1)$, and $\pm(-\frac{\sqrt{3}}{2},\frac{1}{2},1)$, which have no bridging oxygen and As pairs, are negligible. The calculated hopping integrals exceeding 10 meV are given in Table III. We see that those to third-nearest neighbors dominate those to second- and first-nearest neighbors.

The Ni $3d(e_g)$ Wannier orbitals in $NiAs_2O_6$ are similar to the Pd $4d(e_g)$ Wannier orbitals in $PdAs_2O_6$, except that they are more localized. This is consistent with the 1.4 times smaller $3d(e_g)$-band width. Concomitantly, the hopping integrals for $NiAs_2O_6$ listed in parentheses in Table III are about 1.4 times larger than those for $PdAs_2O_6$.

The magnetic exchange interaction, J, can be expressed in general as a sum of antiferromagnetic and ferromagnetic contributions. In the limit of large Coulomb correlation, typically valid for late transition-metal elements like Pd or Ni, the antiferromagnetic contribution is related to the hopping integral t by the second-order perturbation relation $J \sim \frac{t^2}{U}$, where U is the effective on-site Coulomb repulsion defined for the Wannier orbitals. Considering the hopping integrals in Table III, the contribution from the t^2 term in the magnetic exchange gives rise to a factor 2 difference between the Pd and Ni compounds. The estimate of U, unlike that of the hopping

TABLE III. Hopping integrals between Wannier e_g orbitals centered on Pd (or Ni). Hoppings are in meV, and those exceeding 10 meV are listed. Only hoppings between second-nearest neighbors, $d_2 = 4.82$ (4.76) Å, and between third-nearest neighbors, $d_3 = 6.71$ (6.51) Å, are significant.

Vector from m to m' → m,m' ↓	$\pm(0,1,0)$	$\pm\left(\frac{\sqrt{3}}{2},\frac{1}{2},0\right)$	$\pm\left(\frac{\sqrt{3}}{2},-\frac{1}{2},0\right)$	$\pm(0,1,1)$	$\pm\left(\frac{\sqrt{3}}{2},\frac{1}{2},-1\right)$	$\pm\left(\frac{\sqrt{3}}{2},-\frac{1}{2},1\right)$
$3z^2 - r^2, 3z^2 - r^2$	33 (24)			−139 (−99)	−38 (−27)	−38 (−27)
$x^2 - y^2, x^2 - y^2$	−12 (−12)	22 (15)	22 (15)		−106 (−76)	−106 (−76)
$3z^2 - r^2, x^2 - y^2$		−19 (−16)	19 (16)		58 (42)	−58 (−42)

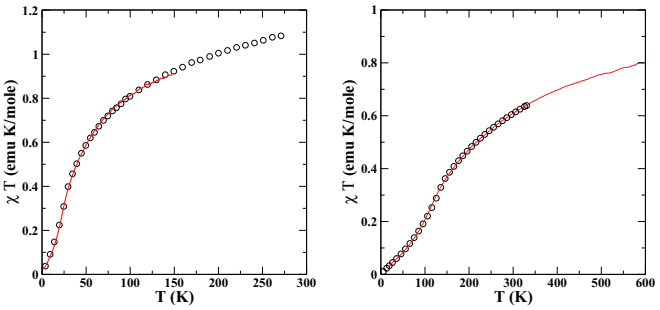

FIG. 8. (Color online) Temperature dependence of the magnetic susceptibility (multiplied by temperature) for $NiAs_2O_6$ (left panel) and $PdAs_2$ O_6 (right panel). The circles correspond to experimental data (taken from Ref. 3 for $NiAs_2O_6$), and the solid lines correspond to calculated data based on the model described in the text.

integral t, is a rather delicate issue. In principle, one should compute U for the Wannier orbitals shown in Fig. 7. However, lacking a prescription to do so, we computed the U values corresponding to Ni-d and Pd-d partial waves, which were truncated outside the atomic spheres defined around an Ni or Pd site. The calculations were carried out within the framework of the constrained DFT scheme.[16–18] The U values calculated in this way were $U_{\mathrm{Pd}} = 5.7$ eV and $U_{\mathrm{Ni}} = 8.4$ eV. But since the Wannier e_g orbitals are far more delocalized than the truncated partial waves, and more so for Pd than for Ni, these U values should be significantly reduced, and more so for Pd than for Ni. This could conceivably lead to the factor $U_{\mathrm{Ni}}/U_{\mathrm{Pd}} \sim 2.4$ needed to bring our theoretical t^2/U estimate for the Néel temperatures of the two compounds into agreement with the measured ratio of 4.7.

C. Spin model and susceptibility

Taking into account only the dominant hopping integrals provided by the N MTO-downfolding calculation, a spin model can be defined in terms of the six pairs of third-nearest-neighbor magnetic interactions, all of size J_3, obtained by summing over the squares of the e_g hopping integrals between the third-nearest neighbors. Based on this model, we have calculated the magnetic susceptibility by considering the following spin-1 Hamiltonian:

$$H = J_3 \sum_{k=0}^{m-1} \sum_{j=0}^{m-1} \sum_{i=0}^{m-1} (S_{i,j,k} S_{i,j+1,k+1} + S_{i,j,k} S_{i+1,j,k+1} + S_{i,j,k} S_{i+1,j+1,k-1}).$$

This model was solved by the quantum Monte Carlo method[19] on a $10 \times 10 \times 10$ lattice. The primary interaction J_3 and the effective Landé g factors were obtained by fitting to the experimental susceptibility. As shown in Fig. 8, the calculated and measured susceptibilities agree very well. The optimal values of the g factor and the exchange parameter J_3 were found to be 2.38 and 62 K for the Pd compound and 2.48 and 13 K for the Ni compound, respectively. We find that the g factors are larger than the spin-only value of 2, in agreement with the discussion in Sec. II C above. The fit of the susceptibilities yields a value of 5 for the ratio of the predominant magnetic exchange parameters of $PdAs_2O_6$ and $NiAs_2O_6$, in good agreement with the ratio of the magnetic transition temperatures.

IV. CONCLUSIONS

Using a combination of susceptibility and neutron diffraction measurements, we have developed a comprehensive experimental description of the magnetic properties of the newly synthesized antiferromagnet $PdAs_2O_6$. Density-functional theory has provided a detailed understanding of the magnetic bond network of this compound, as well as a semiquantitative explanation of the large enhancement of the magnitude of its primary exchange interaction parameters compared to its $3d$ homologue $NiAs_2O_6$. This approach may prove useful for research on other Pd compounds, including the recently discovered[20] ferromagnet PdS_2O_7, and for comparative studies of materials with $4d$ valence electrons and their $3d$-electron counterparts in general.

ACKNOWLEDGMENTS

We are grateful to the referee for constructive criticism, to M. Hölzel and A. Senyshyn for help with the neutron diffraction measurements at the FRM-II, and to O. Jepsen for performing the U calculations. T.S.D. and O.K.A. acknowledge the MPG-India partner group program and the INDO-EU research network RP7 MONAMI for support.

*Present address: Aliah University, DN-41, Sector-V, Salt Lake, Kolkata 700091, India.

[1] D. Orosel and M. Jansen, Z. Anorg. Allg. Chem. **632**, 1131 (2006).
[2] For a recent review, see M. Serafin and B. G. Müller, Z. Anorg. Allg. Chem. **633**, 2523 (2007).
[3] A. M. Nakua and J. E. Greedan, J. Solid State Chem. **118**, 402 (1995).
[4] J. Rodríguez-Carvajal, Physica B **192**, 55 (1993).
[5] V. F. Sears, in *International Tables of Crystallography*, edited by A. J. C. Wilson (Kluwer, Dordrecht, 1992), Vol. C, p. 383.
[6] P. J. Brown, in *International Tables of Crystallography* (Ref. 5), Vol. C, p. 391.
[7] W. J. Moore and L. Pauling, J. Am. Chem. Soc. **63**, 1392 (1941).
[8] M. Weil, Acta Crystallogr. Sec. E **57**, i22 (2001).
[9] R. D. Shannon, Acta Crystallogr. Sec. A **32**, 751 (1976).
[10] J. Rossat-Mignaud, in *Methods of Experimental Physics*, edited by K. Sköld and D. L. Price (Academic, New York, 1987), Vol. 23, p. 69.
[11] M. T. Hutchings and E. J. Samuelsen, Phys. Rev. B **6**, 3447 (1972).
[12] U. von Barth and L. Hedin, J. Phys. C **5**, 1629 (1972).

[13]O. K. Andersen and O. Jepsen, Phys. Rev. Lett. **53**, 2571 (1984).
[14]V. I. Anisimov, I. V. Solovyev, M. A. Korotin, M. T. Czyzyk, and G. A. Sawatzky, Phys. Rev. B **48**, 16929 (1993).
[15]O. K. Andersen and T. Saha-Dasgupta, Phys. Rev. B **62**, R16219 (2000).
[16]P. H. Dederichs, S. Blügel, R. Zeller, and H. Akai, Phys. Rev. Lett. **53**, 2512 (1984).
[17]O. Gunnarsson, O. K. Andersen, O. Jepsen, and J. Zaanen, Phys. Rev. B **39**, 1708 (1989).
[18]V. I. Anisimov, J. Zaanen, and O. K. Andersen, Phys. Rev. B **44**, 943 (1991).
[19]A. W. Sandvik, Phys. Rev. B **59**, R14157 (1999).
[20]J. Bruns, M. Eul, R. Pöttgen, and M. S. Wickleder, Angew. Chem. **124**, 2247 (2012).